



Article

Solid-State Formation of a Potential Melphalan Delivery Nanosystem Based on β -Cyclodextrin and Silver Nanoparticles

Rodrigo Sierpe ^{1,2,3}, Orlando Donoso-González ^{1,2,4,5}, Erika Lang ¹, Michael Noyong ⁵, Ulrich Simon ⁵, Marcelo J. Kogan ^{2,4,*} and Nicolás Yutronic ^{1,*}

¹ Departamento de Química, Facultad de Ciencias, Universidad de Chile, Las Palmeras #3425, Ñuñoa, Santiago 7800003, Chile

² Departamento de Química Farmacológica y Toxicológica, Facultad de Ciencias Químicas y Farmacéuticas, Universidad de Chile, Sergio Livingstone #1007, Independencia, Santiago 8380492, Chile

³ Departamento de Química, Facultad de Ciencias Naturales, Matemática y del Medio Ambiente, Universidad Tecnológica Metropolitana (UTEM), Las Palmeras 3360, Ñuñoa, Santiago 7800003, Chile

⁴ Advanced Center for Chronic Diseases (ACCDiS), Sergio Livingstone #1007, Independencia, Santiago 8380492, Chile

⁵ Institute of Inorganic Chemistry, RWTH Aachen University, Landoltweg 1a, D-52074 Aachen, Germany

* Correspondence: mkogan@ciq.uchile.cl (M.J.K.); nyutroni@uchile.cl (N.Y.)

Abstract: Melphalan (Mel) is an antineoplastic widely used in cancer and other diseases. Its low solubility, rapid hydrolysis, and non-specificity limit its therapeutic performance. To overcome these disadvantages, Mel was included in β -cyclodextrin (β CD), which is a macromolecule that increases its aqueous solubility and stability, among other properties. Additionally, the β CD–Mel complex has been used as a substrate to deposit silver nanoparticles (AgNPs) through magnetron sputtering, forming the β CD–Mel–AgNPs crystalline system. Different techniques showed that the complex (stoichiometric ratio 1:1) has a loading capacity of 27%, an association constant of 625 M^{-1} , and a degree of solubilization of 0.034. Added to this, Mel is partially included, exposing the NH_2 and COOH groups that stabilize AgNPs in the solid state, with an average size of $15 \pm 3 \text{ nm}$. Its dissolution results in a colloidal solution of AgNPs covered by multiple layers of the β CD–Mel complex, with a hydrodynamic diameter of 116 nm, a PDI of 0.4, and a surface charge of 19 mV. The in vitro permeability assays show that the effective permeability of Mel increased using β CD and AgNPs. This novel nanosystem based on β CD and AgNPs is a promising candidate as a Mel nanocarrier for cancer therapy.

Keywords: melphalan; cyclodextrin; silver nanoparticle; inclusion complex; drug delivery; solid-state formation; nanomaterial; sputtering



Citation: Sierpe, R.;

Donoso-González, O.; Lang, E.; Noyong, M.; Simon, U.; Kogan, M.J.; Yutronic, N. Solid-State Formation of a Potential Melphalan Delivery Nanosystem Based on β -Cyclodextrin and Silver Nanoparticles. *Int. J. Mol. Sci.* **2023**, *24*, 3990. <https://doi.org/10.3390/ijms24043990>

Academic Editors: Miguel A. Esteso and Carmen M. Romero

Received: 9 January 2023

Revised: 5 February 2023

Accepted: 8 February 2023

Published: 16 February 2023



Copyright: © 2023 by the authors. Licensee MDPI, Basel, Switzerland. This article is an open access article distributed under the terms and conditions of the Creative Commons Attribution (CC BY) license (<https://creativecommons.org/licenses/by/4.0/>).

1. Introduction

Melphalan (Mel) is a bifunctional alkylating agent widely used at the clinical level in the treatment of multiple types of cancer and other diseases [1–4]. The effectiveness of killing cancer cells of this drug is based on the ability to react extensively with DNA, RNA, and proteins to form interstrand DNA crosslinks, inducing multiple kinds of molecular lesions [5–7]. Nevertheless, Mel presents serious therapeutic disadvantages related to its non-specificity, the resistance of tumor cells, and the need for increasingly higher doses during treatment, generating adverse effects that include leukopenia, mucositis, and diarrhea [8,9]. In this sense, the administration of Mel could be optimized using nanotechnology [10–17]. Specifically, silver nanoparticles (AgNPs) have been used for the loading and transport of antitumor drugs, showing a synergistic effect with these drugs and a site-specific action, which would reduce the administered dose and even reduce the toxicity in healthy cells [18–20]. This research field is controversial; therefore, it is necessary to expand on this point.

The properties of AgNPs intrinsically depend on their size, shape, and surface coating; therefore, if properly designed, they can be used in cancer therapy [21,22]. AgNPs accumulate specifically at tumor sites due to the enhanced permeation and retention effect (called EPR effect); this allows drug targeting if it acts as a nanocarrier [23,24]. In addition to the therapeutic effect of the material itself, which has demonstrated antiproliferative activity against tumor cells of different types [25,26]. On the other hand, due to their excellent optoelectronic properties, they exhibit a localized surface plasmon resonance that allows for photothermal therapy [21,27]. This consists of the conversion of the irradiated energy on these nanoparticles into local heat, which triggers hyperthermia and release of the bound therapeutic material [28–30]; this is especially relevant for the treatment of tumors, for example, one generated by skin cancer, where the therapy must operate on the most external layers of the tissue [31–33]. Likewise, the therapy based on Mel laser irradiation has also been studied by some authors with favorable results on organ transplantation [34–36].

Although Mel vectorization on AgNPs could optimize their transport and synergize at the therapeutic level, solubility and stability in water remain an issue. Current formulations must be prepared in situ as hydrolysis decomposes Mel into a non-active molecule completely within 8 h at 37 °C [37]. In addition, the poor aqueous solubility, less than 1 mg/mL, severely limits the dose administered [3,4,9]. In this sense, a promising approach to overcome these limitations has been the loading of this type of drug into β -cyclodextrin (β CD), forming inclusion complexes [38–40]. β CD is a cyclic oligosaccharide macromolecule, approved by FDA (Food and Drug Administration), composed of 7 glucose units polymerized that have a shape similar to a truncated cone. The use of β CD has a wide range of applications ranging from pharmaceutical formulations, food products, and cosmetics, among others. It has a hydrophobic interior and a hydrophilic exterior that allows non-polar molecules of certain dimensions to be included in its interior, forming a stable complex, preventing hydrolysis, and increasing solubility [41,42]. In general, the toxicity of cyclodextrins depends on the route of administration; by the oral route, they are practically non-toxic; by the parenteral route, they are considered safe; however, increasingly higher doses and their accumulation could be harmful, although if it is administered intravenously, they rapidly disappear from the systemic circulation and are excreted via the kidneys [39,43]. Notably, the inclusion of Mel in cyclodextrin derivatives has been studied, with encouraging results regarding toxicity, stability, and solubility of the unloaded drug [44–46]. In recent years, a research line on cyclodextrin–drug complexes combined with plasmonic nanoparticles has been developed with promising results. The crystals formed by the drug included in the macromolecule acquire an arrangement that allows the stabilization of gold nanoparticles in the solid state, creating new nanosystems with optimal release and performance parameters [13–15,17,47]. A solid formulation containing the drug is a strategy that could optimize its physicochemical properties, such as chemical and physical stability, solubility, and bioavailability, among others. In addition, it allows the development of formulations for different routes of administration, which is especially relevant for Mel.

In this work, two tools were combined synergistically aimed at optimizing the use of Mel in chemotherapy. First, the β CD matrix was used to form the β CD–Mel complex in a solid state. Subsequently, AgNPs were formed and immobilized directly on these crystals by the physical method of magnetron sputtering, thus avoiding the use of agents considered toxic for biomedical applications. Finally, the system was solubilized to obtain a colloidal solution of AgNPs covered by the complex. A schematic representation of the nanosystem formation process at each stage is shown in Figure 1. During its development, this new β CD–Mel–AgNPs crystalline system was characterized using techniques such as powder X-ray diffraction, one and two-dimensional NMR, UV-vis spectroscopy, and scanning electron microscopy. Then, the β CD–Mel crystals with AgNPs on their surface were dissolved, forming the new β CD–Mel–AgNPs colloidal nanosystem, which was characterized using dynamic light scattering, zeta potential, and transmission electron microscopy. The study of relevant pharmaceutical parameters, such as association constant, loading capacity, and

nanosystem size, among others, were included. In addition, the effective permeability of Mel in β CD and with AgNPs was evaluated in an *in vitro* membrane model. Our research is the first report of Mel complexation in β CD and its interaction with AgNPs in a solid state and surfactant-free, where both components work to solve some therapeutic drawbacks of this drug and as a potential nanocarrier.

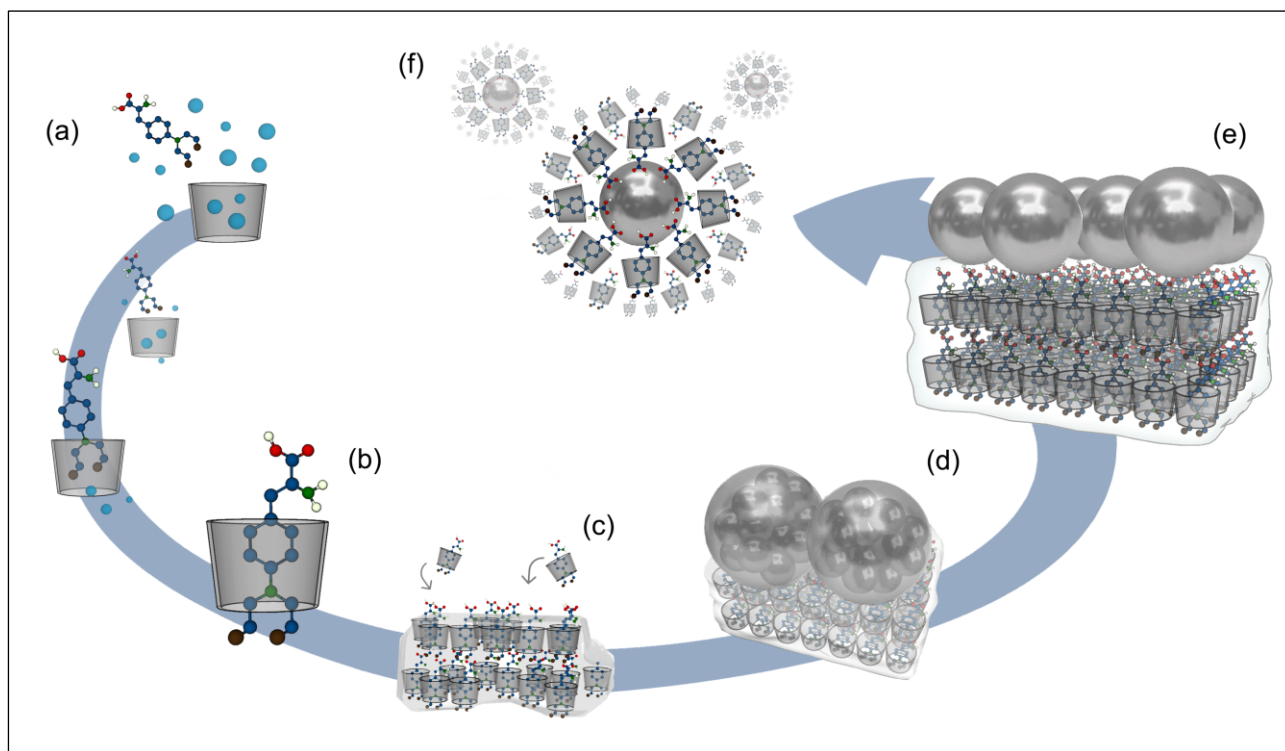


Figure 1. Schematic representation of nanosystem formation: inclusion process of the drug in β CD (a,b), formation of the crystals (c), obtaining and stabilization of AgNPs by magnetron sputtering (d), formation of the β CD–Mel–AgNPs crystalline system, (e) and solubilization process forming the β CD–Mel–AgNPs colloidal nanosystem (f).

2. Results and Discussion

2.1. Formation of the Complex in Solid State

The diffraction patterns of the β CD, Mel, and the complex formed were obtained using PXRD (see Figure 2). The formation of the complex in the solid state causes the disappearance of the Mel peaks, especially in the region above $25^\circ 2\theta$, maintaining a peak corresponding to β CD at 2θ angle of approximately 12° . The crystal packing arrangement of the complex was different from that of its pure species and represents a new crystalline phase, confirming the effective inclusion of the drug in the β CD matrix. Three intense peaks were observed at approximately 4° , 12° and $20^\circ 2\theta$ in the β CD–Mel pattern. It has been reported that the formation of complexes with a $P2_1$ -type structure for β CD matrices hosting aromatic rings at 1:1 (host–guest) molar ratios also exhibit three intense peaks at equal locations. In addition, the geometrical arrangement and thus the respective diffraction pattern varies according to the type of molecular structure of the aromatic guest, according to the region partially exposed to the outside of the β CD cavity and to the water molecules contributing to the new crystalline packing [48–50]. Regarding the physical mixture of pure components, (Figure 2d), it was observed that its diffractogram corresponds to a superposition between the traces of the pure species.

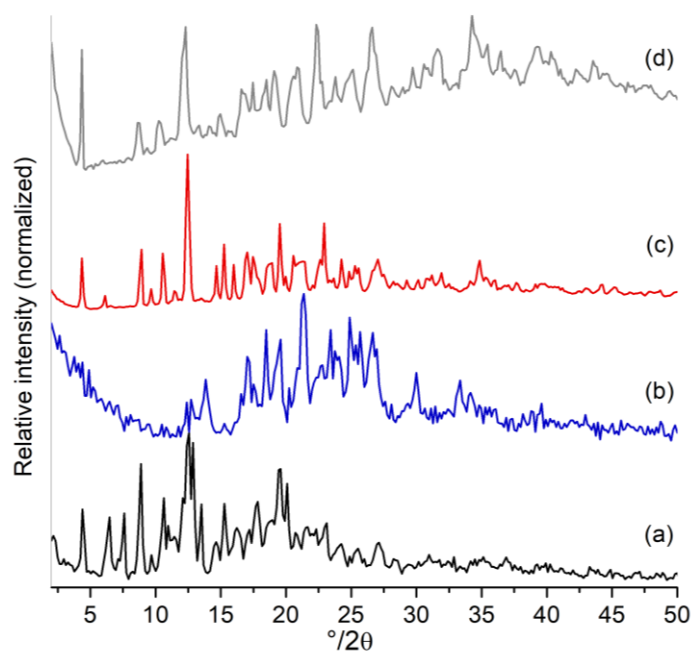


Figure 2. Powder diffractograms of (a) β CD, (b) Mel, (c) β CD–Mel, and (d) physical mixture of β CD and Mel.

2.2. Stability of the Complex in Solution

$^1\text{H-NMR}$ was conducted to study the conformation and stoichiometry of β CD–Mel and to evaluate the stability of Mel included in the complex. The latter was chosen because, in therapy, Mel has poor solubility in water and is unstable on reconstitution and dilution [44]. In 1978, Chang et al. proposed that the hydrolysis of Mel occurs in three phases where chloroethyls, one by one, are transformed into hydroxyethyls by a three-component cyclic intermediate mechanism with the tertiary amine. This process is completed after 8 h [37].

Once the complex was formed in the solid state, it was dissolved, $^1\text{H-NMR}$ spectrum of β CD–Mel in solution was registered and then compared with the free β CD and Mel spectra (see Figure 3).

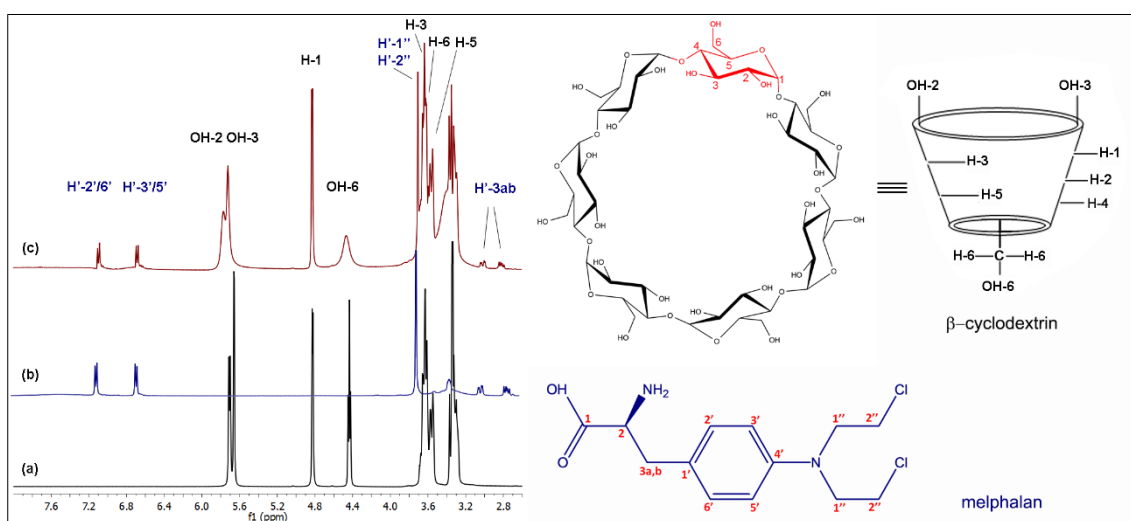


Figure 3. $^1\text{H-NMR}$ spectra of the (a) β CD, (b) Mel, and (c) β CD–Mel complex in DMSO-d_6 .

Table 1 shows the chemical shifts of β CD–Mel compared to its pure species. The shifts of the $2'/6'$, $3'/5'$ protons of the ring and the $1''$ and $2''$ protons of the drug chain towards

lower fields demonstrate interaction with the CD matrix; while the chemical shifts of the H'-3 a and b protons of Mel suggest interactions with the OH groups present on the surface of the β CD cavity. The internal H-3, H-5, and H-6 matrix protons demonstrate that the drug remains included. The OH-6 groups move to higher fields due to the proximity of electronegative groups such as COOH and NH₂ that are close to one of the CD openings. Considering the changes observed in Mel upon hydrolyzing and the signals observed in the spectrum, it is confirmed that through the formation of the complex, the drug can remain stable within the matrix, considerably increasing its applicability in therapy.

Table 1. Chemical shifts of the β CD–Mel complex and free species.

H of β CD	δ β CD (ppm)	δ β CD–Mel (ppm)	$\Delta\delta$ (ppm)	H' of Mel	δ Mel (ppm)	δ β CD–Mel (ppm)	$\Delta\delta$ (ppm)
H-3	3.648	3.653	0.005	H'-1''/2''	3.699	3.702	0.003
H-5	3.555	3.570	0.015	H'-3a	2.736	2.814	0.078
H-6	3.617	3.625	0.006	H'-3b	3.017	3.012	−0.005
OH-2	5.735	5.766	0.031	H'-2'/6'	7.087	7.093	0.006
OH-3	5.680	7.719	0.039	H'-3'/5'	6.671	6.683	0.012
OH-6	4.479	4.464	−0.015				

Integrating the proton signals of β CD and Mel in the ¹H-NMR spectrum of the complex allowed for the determination of the host:guest stoichiometric ratio in solution, according to a methodology used for different CD complexes [51,52]. The integrations of the H-1 proton of the β CD with H'-2'/6' and H'-3'/5' protons of the aromatic ring of Mel were compared. The results show that the complex was formed in a 1:1 stoichiometric ratio, being relevant for potential applications (more details are given in the Supplementary Materials, Section S1).

2.3. Drug Loading and Complexation Efficiency

In pharmaceutical concepts, knowing the stoichiometric ratio allows us to obtain important parameters for potential formulation production [13–16,53]. The 1:1 drug/ β CD molar ratio means that the 0.75 g of cyclodextrin can load 0.20 g of drug, so the loading capacity of the matrix was 27%. The solubility of β CD in water is 18.5 g/L [54], so to completely dissolve the inclusion complex, about 40.5 mL is needed, where 200 mg of the drug would be found. This means that the formation of the complex increases the practical solubility of Mel almost five times.

On the other hand, the phase solubility method allows knowing parameters such as the degree of solubilization, association constant, and complexation efficiency [53] (further details of the procedure and figures are provided in the Supplementary Materials, Section S2). Linear increases in the aqueous solubilities of Mel versus β CD used were observed, with a 0.034 degree of solubilization. In general, the recommendable K_a values of drug:CD complexes are between 50 and 2000 M^{−1}, because at values below 50 M^{−1}, the pharmaceutical formulation may be limited by its low stability, not favoring a controlled release, e.g., an early liberation into the blood and not into the desired tissue. On the other hand, at high K_a values (>2000 M^{−1}), the ability to release the drug by gradient or by stimulus can be affected by the high degree of inclusion of the drug in the β CD cavity, excessively delaying its pharmacokinetics, among other possible therapeutic drawbacks [55,56]. The K_a of β CD–Mel was 625 M^{−1}, being located in an adequate range, with stable host–guest interactions, which prevent its early release and could allow its delivery to the site of action. Furthermore, the complexation efficiency can be used to probe the feasibility of using cyclodextrins in the formulation of drugs. In the β CD–Mel system, the complexation efficiency value was 0.035, being suitable for a potential formulation based on this complex.

2.4. Molecular Interaction and Geometry of the Inclusion Complex

Whereas the formation, stability, and loading parameters of Mel on the complex were in the desired range, for the formation of the nanovehicle by stabilizing AgNPs directly on its surface using β CD, it was necessary to know the availability of adequate exposed functional groups. The rotational overhauser enhancement spectroscopy (ROESY) technique enables observation of interactions between hydrogen nuclei of non-chemically bonded

structures separated by a maximum distance of 5 Å; therefore, it is possible to determine in solution the geometrical structure of supramolecular complexes accurately [51,52]. The ROESY spectra of the β CD–Mel complex are shown in Figure 4a,b. A model showing the proposed geometry of β CD–Mel is shown in Figure 4c (full ROESY spectra are shown in the Supplementary Materials, Section S3).

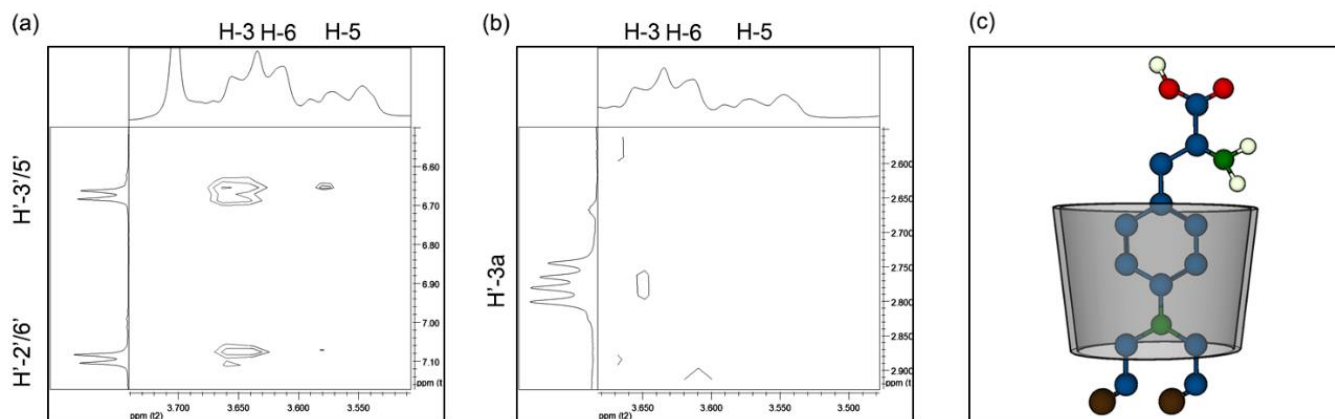


Figure 4. ROESY spectra of the interaction between (a) $H'-2'/6'$ and $H'-3'/5'$ of Mel and H-3, H-6, and H-5 of β CD; (b) $H'-3a$ of Mel and H-3, H-6, and H-5 of β CD in β CD–Mel complex in $DMSO-d_6$; (c) molecular schematic of the proposed inclusion geometry for the β CD–Mel system.

The analysis reveals that the $H'-2'/6'$ and $H'-3'/5'$ protons, corresponding to the aromatic ring of Mel, exhibit a correlation with the H-3 and H-5 protons of β CD (Figure 4a). This indicates that the aromatic ring is located in the wider region of the matrix. The exact orientation of the drug can be elucidated from the cross-peaks observed between the internal protons of β CD with the $H'-3a$ proton of Mel (Figure 4b). This reveals that Mel is exposed toward the major opening, and thus, the chloroethyl chains are oriented toward the minor opening of the matrix. These results explain the chemical shifts of Mel in the 1H -NMR spectrum, where shifts towards lower fields of the OH-6 and the $H'-1''$ and $H'-2''$ protons were observed. This confirms that it is the interaction of the primary hydroxyl groups of β CD with the chloroethyl chains of Mel that causes this effect. Accordingly, by the dimensions of both molecules, the NMR and ROESY result strongly suggests that the COOH and NH_2 functional groups of Mel are oriented outside the cavity of the matrix, thus making it a suitable candidate to stabilize AgNPs.

2.5. Deposition of Silver Nanoparticles on the β cyclodextrin–Melphalan Complex

AgNPs were obtained and deposited using the physical method of magnetron sputtering in vacuum. The technique consists of the detachment of atoms from a thin metallic film, which agglomerate and stabilize on a substrate, reaching a nanometric size [13–15,57,58]. As we have confirmed, Mel was partially included within β CD, exposing the amine and carboxylic acid functional groups towards one of its openings. This arrangement allowed the solid-state complexes to act as substrates and the crystalline faces that expose these functional groups to interact specifically with silver atoms allowing its accumulation, forming, and stabilizing nanoparticles. Figure 5a shows a schematic representation of this process. The new β CD–Mel–AgNPs crystalline system was characterized using UV-vis diffuse reflectance spectroscopy, SEM, EDX, and FE-SEM. Figure 5b corresponds to the absorbance spectra of AgNPs deposited on the β CD–Mel complexes. The maximum absorbance peak in the SPR of the nanoparticles was located at 450 nm (see the UV-vis spectra of Mel in solid state in the Supplementary Materials, Section S4).

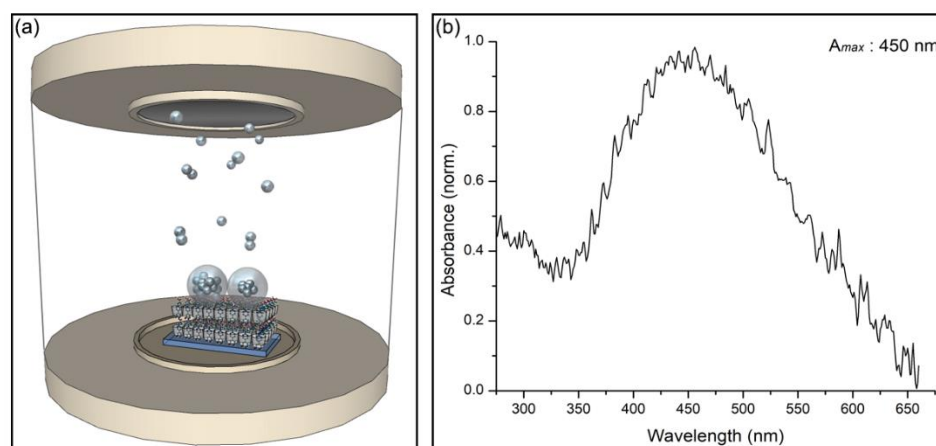


Figure 5. (a) Scheme of the release of atoms and formation of AgNPs on crystals of the β CD–Mel complex from the cathodic sputtering of a metal foil; (b) absorbance spectra of AgNPs deposited on β CD–Mel using magnetron sputtering.

It has been reported that AgNPs with an average diameter of 10 nm show an SPR with a maximum absorbance peak at 400 nm [59]. There are reports of AgNPs formation on different substrates using this method. In these studies, it is argued that the bathochromic shift of the band above 400 nm is probably due to an increase in the size of the formed nanoparticles (above 10 nm), to the change in the dielectric environment or to an interparticle plasmon coupling [57,60–62].

Figure 6 corresponds to SEM images showing directly the nanoparticles deposited on crystals of the complex, together with an elemental analysis performed on a section of the crystal using EDX (see more FE-SEM images and EDX table information in Supplementary Materials, Section S5).

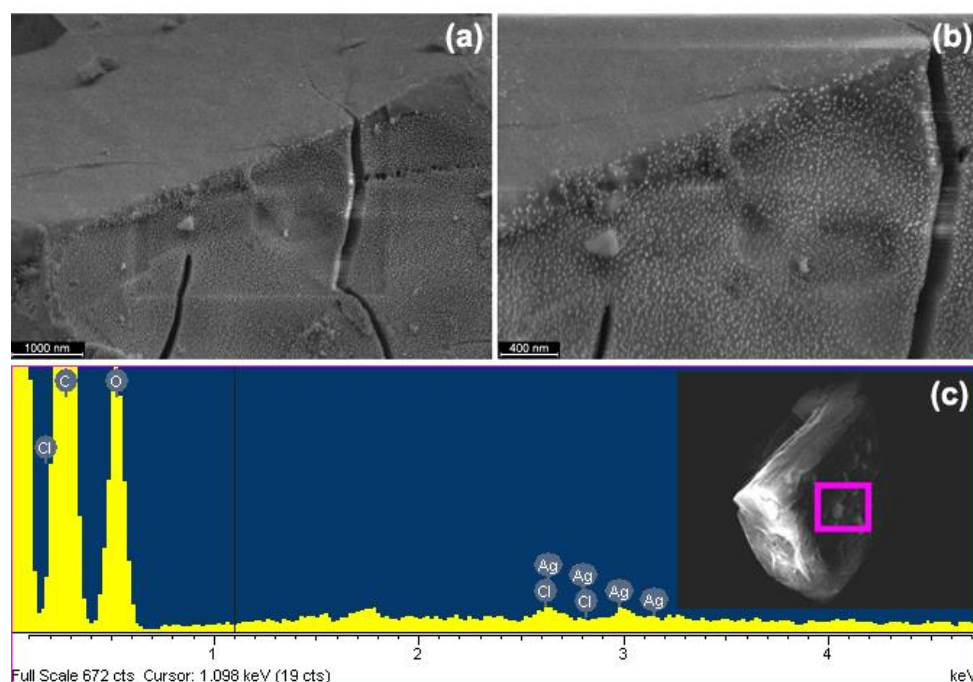


Figure 6. (a,b) FE-SEM micrograph of β CD–Mel with AgNPs, the time of exposure in sputtering was 32 s. (c) EDX spectrum taken at the marked area in the SEM micrograph at its right side of AgNPs deposited on β CD–Mel by sputtering, with elemental analysis values in the inset.

The phenomenon of the inclusion of molecules on β CD generates crystalline arrangements different from that of their pure species. In this case, it was observed that the crystalline morphology of the β CD–Mel complex is different with respect to the pure compounds β CD and Mel (see SEM images information in Supplementary Materials, Section S6).

This corroborates what was previously discussed in the analysis of the samples by XRD. Figure 6a,b shows a high concentration of AgNPs of homogeneous size, preferentially accumulated on one side of the crystal, where NH_2 and COOH functional groups of Mel are exposed, allowing its stabilization and confirming that the phenomenon of aggregation is widely suppressed. The EDX spectra obtained from the surface area analyzed show the atomic and weight elemental composition of the sample (see Figure 6c). The main components were carbon and oxygen; chlorine is also included, coming from the drug, and silver from the nanoparticles that remain stable in the solid state on the surface of the crystals.

2.6. Formation of β cyclodextrin–Melphalan–Silver Nanoparticles Nanosystem

The β CD–Mel crystals with deposited AgNPs were solubilized in water, promoting the formation of a colloidal solution of AgNPs stabilized by the β CD–Mel complex, as schematized in Figure 7a. The new β CD–Mel–AgNPs colloidal nanosystem was characterized by DLS, zeta potential, and TEM. The results are summarized in Table 2.

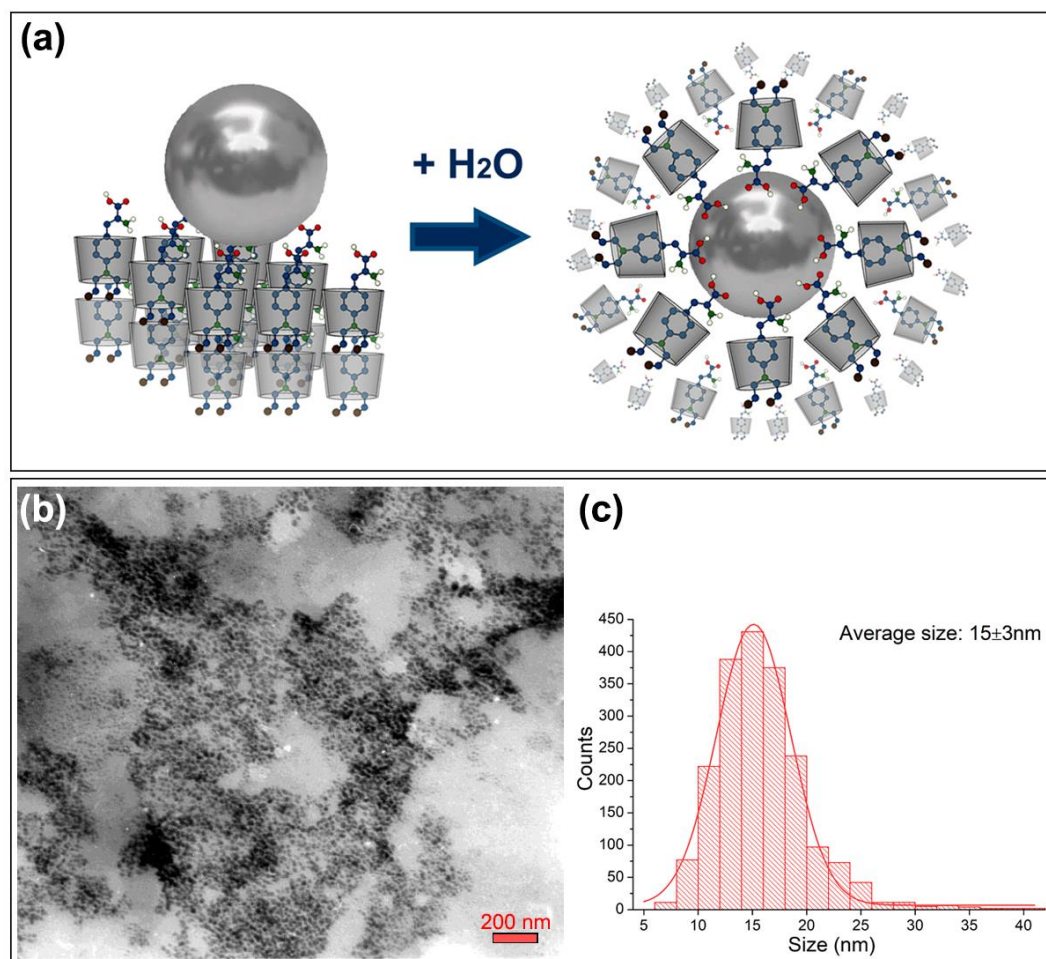


Figure 7. (a) Schematic representation of the solubilization process of AgNPs onto β CD–Mel crystalline complex forming the β CD–Mel–AgNPs nanosystem in colloidal solution, (b) TEM micrograph of β CD–Mel–AgNPs colloidal nanosystem with its respective size distribution histogram (c).

Table 2. Hydrodynamic diameter, polydispersity index (PDI), zeta potential, and TEM size of β CD–Mel–AgNPs colloidal nanosystem.

System	Hydrodynamic Diameter (nm)	PDI	Zeta Potential (mV)	TEM Size (nm)
β CD–Mel–AgNPs	116 \pm 63	0.40	19 \pm 5	15 \pm 3

The solvation sphere diameter of the nanosystem was 116 nm with a polydispersity of 0.4, characteristic of β CD-based nanosystems [12,16,17,63–65]. Therefore, the dissolution process causes the metal nanoparticles to be surrounded by multiple layers of the complex, as has been previously reported for analogous nanosystems using gold nanoparticles [13–15]. In addition, the drug remains partially included in the cavity of the β CD, and its functional groups interact with the surface of Ag atoms. The above was confirmed by the positive surface charge of the β CD–Mel–AgNPs colloidal nanosystem, which was attributed to the NH_2 groups of Mel [66–68]. The size of spherical AgNPs was determined using micrographs obtained by TEM (see Figure 7b). A high concentration of AgNPs very close to each other was observed, homogeneous in size and shape, mostly in the range of 10 to 20 nm. Through the analysis of the respective histogram, an average diameter of 15 \pm 3 nm was reported. The difference between the TEM size and the hydrodynamic diameter is explained by the multiple layers of β CD–Mel, which cover the nanoparticles and maintain the stability of the colloid. Interestingly, for metal nanoparticles above 5 nm, the size is not a critical parameter in the toxicity profile of a nanosystem, since it has no disruptive effects on healthy cells and can be rapidly excreted by the body [24,69]. Once they accumulate in fenestrated tissue, such as tumors, the expected long-term toxicity of AgNPs is due to the oxidative release of Ag^+ that could act synergistically for potential treatment [26]. Accordingly, the average size of the nanoparticles and the hydrodynamic diameter of the β CD–Mel–AgNPs colloidal nanosystem now open the way to possible applications in therapy, in addition to being a stable nanocarrier for Mel. In this sense, one of the relevant tests to validate this new system as a nanocarrier in solution is to evaluate its permeability in membranes. For this, studies using the PAMPA method were performed.

2.7. Permeability Assays on Artificial Membranes

The PAMPA method is used to predict the passive permeability of biologically relevant species, such as drugs, across the membrane. The assay is performed on a donor and acceptor plate, in which the ability of a compound to diffuse between the two plates separated by a phosphatidylcholine filter is measured, which acts as a lipid membrane and simulates the lipid bilayer of different types of cells. Since artificial membranes do not contain active transport systems, only passive diffusion can be studied [70,71]. Cyclodextrins can enhance the permeability of drugs through an artificial membrane under certain conditions. However, cyclodextrin-based complexes increase the total amount of drug in the solution and the concentration gradient. The molecule excess can decrease penetration, especially lipophilic drugs that could permeate the membrane. Other factors such as agitation speed, pH, type of cyclodextrin, or the association constant of each inclusion complex are variables to be considered [72,73].

Figure 8 shows the effective permeability of Mel, β CD–Mel complex, and β CD–Mel–AgNPs colloidal nanosystem analyzed by PAMPA. The controls used behaved as expected, indicating that the membranes were well constructed. In the case of Mel, as part of the complex, its effective permeability increased with respect to Mel alone, which was consistent with the role of β CD, maintaining drug stability and, in turn, altering membrane properties [74,75]. In addition, Mel, in the presence of AgNPs, also increases its effective permeability with respect to Mel alone, probably because the colloid is surrounded by multiple layers of the β CD–Mel complex [76,77]; however, it does not exceed the permeability of the complex. This is explained by the interaction of the NH_2 functional group of Mel with the surface of the AgNPs, decreasing their migration into the membrane. The foregoing suggests that AgNPs maintain the stability and composition of the nanosystem under the experimental conditions studied, which qualifies the system as a promising candidate for

site-directed drug transport [18,26,78–80] since it would avoid its non-specificity or early action in healthy cells during systemic circulation. On the other hand, it conditions the nanocarrier to release the drug through an activation with external stimuli to the biological environment, such as laser irradiation [11,15,17,19,47,81].

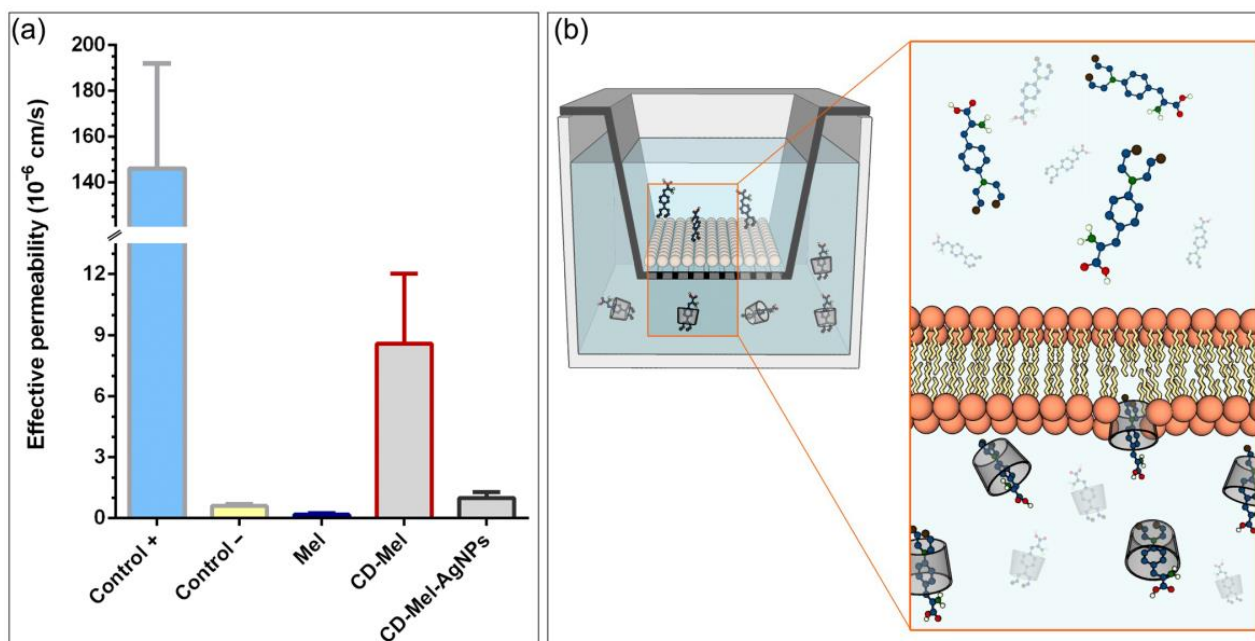


Figure 8. (a) Effective permeabilities of free Mel, Mel included in β CD and Mel in β CD–AgNPs nanosystem. Thiopental and Evans Blue solutions were used as negative and positive controls, respectively. The assays were performed at 37 °C for 24 h, using PBS as solvent, ($n = 3$); (b) representation of a transwell plate used in PAMPA with a scheme of permeation of the drug through an artificial membrane.

3. Materials and Methods

3.1. Reagents and Solvents

In the preparation of the complex, the following reagents were used: β CD hydrate (98%, 1134.98 g/mol), Mel (>95%, 305.2 g/mol), Dimethyl sulfoxide (DMSO)- d_6 (99.99% D, 84.17 g/mol), Phosphatidylcholine (99%), Dodecane (99%, 170.33 g/mol), Phosphate buffered saline (PBS) tablets, Thiopental (99%, 242.34 g/mol), and Evans Blue (75%, 960.81) provided by Sigma-Aldrich (Saint Louis, MO, USA). As solvents, ethanol p.a. and water for chromatography LiChrosolv[®] brand Merck (Darmstadt, Germany) were employed. To obtain the AgNPs via magnetron sputtering, a silver foil of high purity (99.9%) was used as a precursor.

3.2. Synthesis of the β CD–Mel Complex

To synthesize the β CD–Mel complex, the saturated solutions method was employed [13–15,17,82,83]. In total, 0.2025 g of Mel were dissolved in ethanol and then added to a solution of β CD (0.7530 g dissolved in water) at 4 °C with gentle and constant stirring, allowing the temperature to rise slowly up to room temperature. The new solution was kept motionless under a hood for one week until the evaporation of the solvents. Finally, small crystals precipitated at the bottom of the crystallizer were extracted and washed with a 50% *v/v* solution (ethanol/water) at 4 °C and vacuum filtered for one hour in a kitasate with a Büchner funnel equipped with a double layer of filter paper, to remove the excesses of cyclodextrin, drug or solvents that moisten the complex. The crystals were then pulverized and dried in a vacuum line to remove the water or ethanol, which may remain occluded in the powder, then stored in amber vials with a Teflon seal. The new β CD–Mel complex was characterized

by powder X-ray diffraction (PXRD), NMR of one (^1H) and two (ROESY) dimensions, UV-vis spectroscopy for calculating the loading capacity, degree of solubilization, complexation efficiency, and association constant. The complex was also used for a permeability study called PAMPA (parallel artificial membrane permeability assay).

3.3. Formation of Silver Nanoparticles

AgNPs were obtained using magnetron sputtering under a high vacuum, depositing them onto crystalline powder of the βCD -Mel complex acting as a substrate [57,84–86]. In total, approximately 20 mg of this complex was dispersed on a glass slide, which was placed inside the chamber of the equipment, together with a silver foil serving as a cathode. The chamber was evacuated to 0.5 mbar; then, Argon was injected together with a current of 25 mA to ionize the gas, which hit the metal foil, releasing silver atoms that afterward were deposited and stabilized on the complex. The accumulation of atoms on specific crystalline faces of βCD -Mel forms AgNPs in a process that lasts for 20 s. βCD -Mel-AgNPs was characterized by UV-vis spectroscopy, field emission scanning electron microscopy (FE-SEM), energy-dispersive X-ray spectroscopy (EDX), dynamic light scattering (DLS), zeta potential, transmission electronic microscopy (TEM), and PAMPA.

3.4. Powder X-ray Diffraction (PXRD)

The analysis of the complex and pure species βCD and Mel was performed using a Siemens D-5000 diffractometer with graphite-monochromated Cu K- α radiation at 40 kV and 30 mA with a wavelength of 1.540598 Å.

3.5. ^1H -NMR and ROESY

Measurements for the complex and pure species βCD and Mel were performed at 300 K in DMSO- d_6 (99.99%) on a Bruker Advance 400 MHz superconducting NMR spectrometer. All 2D NMR spectra were acquired using pulsed-field gradient-selected methods during a mixing time of 12 h. Additionally, the stoichiometry of the complex was evaluated using the integration of the signals of the protons of βCD and Mel in the spectrum of βCD -Mel.

3.6. Loading Capacity

The loading capacity of the βCD -Mel was calculated from the weights of βCD and drug obtained using Equation (1) [87].

$$\text{Loading capacity} = \frac{\text{Weight of drug in } \beta\text{CD}}{\text{Weight of } \beta\text{CD}} \times 100 \quad (1)$$

3.7. Phase Solubility Studies

Studies were performed following the Higuchi and Connors method [53]. The Beer-Lambert law was used to quantify Mel, considering its absorbance at 301 nm. First, known concentrations (C) of Mel were measured by UV-vis. From the UV-vis spectra, the absorbance maxima at 301 nm (A_{max}) were extracted. The slope from the A_{max} vs. C graph, corresponded to the ϵ of the drug (For details, graphs, and tables, see Supplementary Materials, Section S2). Then, the βCD concentration versus the loaded Mel concentration (calculated by Beer-Lambert law) was plotted. The value of the slope of the graphs related to the amount of βCD added to the amount of solubilized drug, indicating the degree of solubilization. The degree of solubilization was used to calculate the association constant (K_a) and complexation efficiency of the βCD -Mel system using Equations (2) and (3), respectively [16].

$$K_{a(1:1)} = \frac{\text{Degree of solubilization}}{[C_0](1 - \text{Degree of solubilization})} \quad (2)$$

$$\text{Complexation efficiency} = K_{a(1:1)}[C_0] = \frac{\text{Degree of solubilization}}{(1 - \text{Degree of solubilization})} \quad (3)$$

$[C_o]$ corresponds to the concentration of the free drug in the absence of β CD.

3.8. UV-Vis Spectroscopy in Solid State

The AgNPs deposited onto β CD–Mel were characterized using UV-vis spectroscopy in a solid state [88–90]. First, the diffuse reflectance was measured using a Shimadzu UV 2450 spectrophotometer with barium sulfate as a baseline. In addition, the spectrum of the complex was used as a second baseline. Then, the absorbance of the AgNPs was determined using the Kubelka–Munk transformation.

3.9. (Field Emission-) Scanning Electron Microscopy and Energy Dispersive Spectroscopy

SEM images were obtained using an LEO 1420VP equipment with an Oxford 7424 energy dispersive spectrometer coupled at an accelerating voltage of 25 kV. FE-SEM images were obtained using a Zeiss Leo Supra 35-VP at an accelerating voltage of 15 kV and 20 kV.

3.10. Dynamic Light Scattering and Zeta Potential Measurements

Dynamic light scattering and zeta potential measurements were performed at 25 °C using a Zetasizer model Nano ZS. The size distribution of the samples was determined from the results of the intensity distribution values using the cumulant method. The Smoluchowski approximation was used to calculate zeta potentials based on measured electrophoretic mobility.

3.11. Transmission Electron Microscopy

TEM images were obtained using a JEOL JEM 1200 EX II instrument. The samples with AgNPs were prepared by dispersing approximately 0.5 mg in 100 μ L of isopropanol (30%). Then, 20 μ L of the solution was deposited onto a copper grid with a continuous film of Formvar, the excess solution was removed, and the grid was dried. The acceleration voltage used was 80 kV. More than two thousand nanoparticles were counted to produce the size distribution histogram. The average diameter was obtained from the peak of the Gaussian fit performed on the graph.

3.12. Parallel Artificial Membrane Permeability Assay (PAMPA)

The PAMPA studies require two types of well, a donor and an acceptor (Transwell plates); in addition, the acceptor well has a semipermeable membrane of PVDF (polyvinylidene fluoride). On the PVDF membranes were deposited 4.0 μ L of a solution of phosphatidylcholine in dodecane (20 mg/mL) for 5 min until complete evaporation of the organic solvent. Subsequently, 300 μ L of PBS (pH = 7.4) was added. In the donor well were deposited 300 μ L of each sample dissolved in PBS, which are: Mel, β CD–Mel, and β CD–Mel–AgNPs (all concentration data in Supplementary Materials, Section S7). As positive and negative controls, a solution of Thiopental (10 mg in 100 mL of PBS 10 mM) and a solution of Evans Blue (200 mg in 100 mL of PBS 10 mM) were used, respectively. After loading the donor well with the samples and the controls, and the acceptor well with PBS, they were assembled, covered, and sealed using parafilm. Each PAMPA was performed in triplicate ($n = 3$) for 24 h at 37 °C with constant agitation to 280 rpm.

The effective permeability (P_e) was determined by the following formula:

$$P_e = \frac{-218.3}{t} \cdot \log \left[1 - \frac{2 \cdot C_A(t)}{C_D(0)} \right] \cdot 10^{-6} \text{ cm/s} \quad (4)$$

t = measurement time in hours.

C_A = concentration in acceptor plate at time t .

C_D = concentration in donor plate at time zero.

To calculate the concentrations in the acceptor plate, the absorbances of the different plates were measured using a UV-vis spectrophotometer and the respective calibration curve of Mel in PBS [70,71].

4. Conclusions

In summary, a β CD–Mel crystalline solid complex was formed reproducibly in a 1:1 molar ratio. The hydrophobic cavity of β CD allowed the inclusion of Mel, which prevents hydrolysis and subsequent degradation of the drug. The exhaustive characterization of the complex confirmed that Mel partially exposes the $-NH_2$ and $COOH$ functional groups, allowing the crystals to act as a substrate for the stabilization of silver atoms, and the consequent formation of AgNPs using magnetron sputtering. In turn, the solubilization of the β CD–Mel–AgNPs crystalline system generates a colloidal solution, where the AgNPs are covered in multiple layers by the complex. The loading capacity, the stability of the drug, and the association constant of the complex, together with the size achieved of the nanoparticles and the effective permeability examined for β CD–Mel and β CD–Mel–AgNPs are promising results that validate this nanosystem as a new drug nanocarrier for Mel. Accordingly, the effective and stable Mel loading in this new nanosystem based on β CD and AgNPs shows potential as a novel alternative to traditional cancer therapeutics.

As a future perspective, evaluating the synergistic effect of the components of the nanosystem, together with studies of cytotoxicity and laser-triggered controlled release of Mel in *in vitro* and *in vivo* models, are considered necessary to position this nanosystem as a useful tool in drug delivery applied to cancer.

Supplementary Materials: The following supporting information can be downloaded at: <https://www.mdpi.com/article/10.3390/ijms24043990/s1>.

Author Contributions: Conceptualization, R.S., M.J.K. and N.Y.; methodology, R.S., M.N., U.S., M.J.K. and N.Y.; validation R.S., M.N., U.S., M.J.K. and N.Y.; formal analysis, R.S., O.D.-G., E.L. and M.N.; investigation, R.S., M.J.K. and N.Y.; resources, R.S., O.D.-G., U.S., M.J.K. and N.Y.; writing—original draft preparation, R.S. and O.D.-G.; writing—review and editing, R.S., O.D.-G., M.N., U.S., M.J.K. and N.Y.; visualization, R.S. and O.D.-G.; supervision, N.Y. and M.J.K.; project administration, R.S., M.J.K. and N.Y.; funding acquisition, R.S., M.J.K. and N.Y. All authors have read and agreed to the published version of the manuscript.

Funding: This research was funded by: Rodrigo Sierpe gives thanks to the ANID-FONDECYT number 11221289. Orlando Donoso-González gives thanks to the ANID doctoral scholarship (no. 21180548). Marcelo J. Kogan gives thanks to the ANID-FONDECYT number 1211482, Fondecuip EQM170111, and ANID-FONDAP number 15130011.

Institutional Review Board Statement: Not applicable.

Informed Consent Statement: Not applicable.

Data Availability Statement: Not applicable.

Conflicts of Interest: The authors declare no conflict of interest.

References

1. van Kan, M.; Burns, K.E.; Helsby, N.A. A systematic review of inter-individual differences in the DNA repair processes involved in melphalan monoadduct repair in relation to treatment outcomes. *Cancer Chemother. Pharmacol.* **2021**, *88*, 755–769. [CrossRef]
2. Bayraktar, U.D.; Bashir, Q.; Qazilbash, M.; Champlin, R.E.; Ciurea, S.O. Fifty Years of Melphalan Use in Hematopoietic Stem Cell Transplantation. *Biol. Blood Marrow Transplant.* **2013**, *19*, 344–356. [CrossRef]
3. Gregory, W.M.; Richards, M.A.; Malpas, J.S. Combination chemotherapy versus melphalan and prednisolone in the treatment of multiple myeloma: An overview of published trials. *J. Clin. Oncol.* **1992**, *10*, 334–342. [CrossRef]
4. Samuels, B.L.; Bitran, J.D. High-dose intravenous melphalan: A review. *J. Clin. Oncol.* **1995**, *13*, 1786–1799. [CrossRef]
5. Amin, A.M.; Soliman, S.E.; El-Aziz, H.A. Preparation and biodistribution of [125I]Melphalan: A potential radioligand for diagnostic and therapeutic applications. *J. Label. Compd. Radiopharm.* **2010**, *53*, 1–5. [CrossRef]
6. Colvin, M.E.; Quong, J.N. DNA-alkylating events associated with nitrogen mustard based anticancer drugs and the metabolic byproduct Acrolein. *Adv. DNA Seq. Agents* **2002**, *4*, 29–46. [CrossRef]
7. Nath, C.E.; Trotman, J.; Tiley, C.; Presgrave, P.; Joshua, D.; Kerridge, I.; Kwan, Y.L.; Gurney, H.; McLachlan, A.J.; Earl, J.W.; et al. High melphalan exposure is associated with improved overall survival in myeloma patients receiving high dose melphalan and autologous transplantation. *Br. J. Clin. Pharmacol.* **2016**, *82*, 149–159. [CrossRef]

8. Kühne, A.; Tzvetkov, M.V.; Hagos, Y.; Lage, H.; Burckhardt, G.; Brockmöller, J. Influx and efflux transport as determinants of melphalan cytotoxicity: Resistance to melphalan in MDR1 overexpressing tumor cell lines. *Biochem. Pharmacol.* **2009**, *78*, 45–53. [[CrossRef](#)]
9. Sarosy, G.; Leyland-Jones, B.; Soochan, P.; Cheson, B.D. The systemic administration of intravenous melphalan. *J. Clin. Oncol.* **1988**, *6*, 1768–1782. [[CrossRef](#)]
10. Morales-Zavala, F.; Arriagada, H.; Hassan, N.; Velasco, C.; Riveros, A.; Álvarez, A.R.; Minniti, A.N.; Rojas-Silva, X.; Muñoz, L.L.; Vasquez, R.; et al. Peptide multifunctionalized gold nanorods decrease toxicity of β -amyloid peptide in a *Caenorhabditis elegans* model of Alzheimer's disease. *Nanomed. Nanotechnol. Biol. Med.* **2017**, *13*, 2341–2350. [[CrossRef](#)]
11. Real, D.A.; Bolaños, K.; Priotti, J.; Yutronic, N.; Kogan, M.J.; Sierpe, R.; Donoso-González, O. Cyclodextrin-modified nanomaterials for drug delivery: Classification and advances in controlled release and bioavailability. *Pharmaceutics* **2021**, *13*, 2131. [[CrossRef](#)]
12. Donoso-González, O.; Lodeiro, L.; Aliaga, Á.E.; Laguna-Bercero, M.A.; Bollo, S.; Kogan, M.J.; Yutronic, N.; Sierpe, R. Functionalization of gold nanostars with cationic β -cyclodextrin-based polymer for drug co-loading and sers monitoring. *Pharmaceutics* **2021**, *13*, 261. [[CrossRef](#)]
13. Asela, I.; Noyong, M.; Simon, U.; Andrades-Lagos, J.; Campanini-Salinas, J.; Vásquez-Velásquez, D.; Kogan, M.; Yutronic, N.; Sierpe, R. Gold nanoparticles stabilized with β -cyclodextrin-2-amino-4-(4-chlorophenyl) thiazole complex: A novel system for drug transport. *PLoS ONE* **2017**, *12*, e0185652. [[CrossRef](#)]
14. Sierpe, R.; Noyong, M.; Simon, U.; Aguayo, D.; Huerta, J.; Kogan, M.J.; Yutronic, N. Construction of 6-thioguanine and 6-mercaptopurine carriers based on β -cyclodextrins and gold nanoparticles. *Carbohydr. Polym.* **2017**, *177*, 22–31. [[CrossRef](#)]
15. Sierpe, R.; Lang, E.; Jara, P.; Guerrero, A.R.; Chornik, B.; Kogan, M.J.; Yutronic, N. Gold Nanoparticles Interacting with β -Cyclodextrin-Phenylethylamine Inclusion Complex: A Ternary System for Photothermal Drug Release. *ACS Appl. Mater. Interfaces* **2015**, *7*, 15177–15181. [[CrossRef](#)]
16. Asela, I.; Donoso-González, O.; Yutronic, N.; Sierpe, R. β -cyclodextrin-based nanosponges functionalized with drugs and gold nanoparticles. *Pharmaceutics* **2021**, *13*, 513. [[CrossRef](#)]
17. Quintana-Contardo, S.; Donoso-González, O.; Lang, E.; Guerrero, A.R.; Noyong, M.; Simon, U.; Kogan, M.J.; Yutronic, N.; Sierpe, R. Optimizing Dacarbazine Therapy: Design of a Laser-Triggered Delivery System Based on β -Cyclodextrin and Plasmonic Gold Nanoparticles. *Pharmaceutics* **2023**, *15*, 458. [[CrossRef](#)]
18. Sironmani, A.; Daniel, K. Silver Nanoparticles—Universal Multifunctional Nanoparticles for Bio Sensing, Imaging for Diagnostics and Targeted Drug Delivery for Therapeutic Applications. In *Drug Discovery and Development—Present and Future*; Intechopen: London, UK, 2012; pp. 463–487. [[CrossRef](#)]
19. Ivanova, N.; Gugleva, V.; Dobрева, M.; Pehlivanov, I.; Stefanov, S.; Andonova, V. Silver Nanoparticles as Multi-Functional Drug Delivery Systems. In *Nanomedicine*; Intechopen: London, UK, 2019. [[CrossRef](#)]
20. Gomes, H.I.O.; Martins, C.S.M.; Prior, J.A.V. Silver nanoparticles as carriers of anticancer drugs for efficient target treatment of cancer cells. *Nanomaterials* **2021**, *11*, 964. [[CrossRef](#)]
21. Abbasi, E.; Milani, M.; Aval, S.F.; Kouhi, M.; Akbarzadeh, A.; Nasrabadi, H.T.; Nikasa, P.; Joo, S.W.; Hanifehpour, Y.; Nejati-Koshki, K.; et al. Silver nanoparticles: Synthesis methods, bio-applications and properties. *Crit. Rev. Microbiol.* **2016**, *42*, 173–180. [[CrossRef](#)]
22. Prasher, P.; Sharma, M.; Mudila, H.; Gupta, G.; Sharma, A.K.; Kumar, D.; Bakshi, H.A.; Negi, P.; Kapoor, D.N.; Chellappan, D.K.; et al. Emerging trends in clinical implications of bio-conjugated silver nanoparticles in drug delivery. *Colloids Interface Sci. Commun.* **2020**, *35*, 100244. [[CrossRef](#)]
23. Kovács, D.; Igaz, N.; Gopisetty, M.K.; Kiricsi, M. Cancer Therapy by Silver Nanoparticles: Fiction or Reality? *Int. J. Mol. Sci.* **2022**, *23*, 839. [[CrossRef](#)] [[PubMed](#)]
24. Lin, Z.; Monteiro-Riviere, N.A.; Riviere, J.E. Pharmacokinetics of metallic nanoparticles. *Wiley Interdiscip. Rev. Nanomed. Nanobiotechnol.* **2015**, *7*, 189–217. [[CrossRef](#)] [[PubMed](#)]
25. Vlăsceanu, G.M.; Marin, Ș.; Țiplea, R.E.; Bucur, I.R.; Lemnaru, M.; Marin, M.M.; Grumezescu, A.M.; Andronescu, E. Silver nanoparticles in cancer therapy. In *Nanobiomaterials in Cancer Therapy: Applications of Nanobiomaterials*; William Andrew Publishing: Norwich, NY, USA, 2016; pp. 29–56. ISBN 9780323428866.
26. Mathur, P.; Jha, S.; Ramteke, S.; Jain, N.K. Pharmaceutical aspects of silver nanoparticles. *Artif. Cells Nanomed. Biotechnol.* **2018**, *46*, 115–126. [[CrossRef](#)] [[PubMed](#)]
27. Austin, L.A.; MacKey, M.A.; Dreaden, E.C.; El-Sayed, M.A. The optical, photothermal, and facile surface chemical properties of gold and silver nanoparticles in biondiagnostics, therapy, and drug delivery. *Arch. Toxicol.* **2014**, *88*, 1391–1417. [[CrossRef](#)]
28. Shipunova, V.O.; Belova, M.M.; Kotelnikova, P.A.; Shilova, O.N.; Mirkasymov, A.B.; Danilova, N.V.; Komedchikova, E.N.; Popovtzer, R.; Deyev, S.M.; Nikitin, M.P. Photothermal Therapy with HER2-Targeted Silver Nanoparticles Leading to Cancer Remission. *Pharmaceutics* **2022**, *14*, 1013. [[CrossRef](#)]
29. Bose, P.; Priyam, A.; Kar, R.; Pattanayak, S.P. Quercetin loaded folate targeted plasmonic silver nanoparticles for light activated chemo-photothermal therapy of DMBA induced breast cancer in Sprague Dawley rats. *RSC Adv.* **2020**, *10*, 31961–31978. [[CrossRef](#)]
30. Behnam, M.A.; Emami, F.; Sobhani, Z.; Koochi-Hosseiniabadi, O.; Dehghanian, A.R.; Zebarjad, S.M.; Moghim, M.H.; Oryan, A. Novel combination of silver nanoparticles and carbon nanotubes for plasmonic photo thermal therapy in melanoma cancer model. *Adv. Pharm. Bull.* **2018**, *8*, 49–55. [[CrossRef](#)]

31. El-Hussein, A. Study DNA Damage after Photodynamic Therapy using Silver Nanoparticles with A549 cell line. *J. Nanomed. Nanotechnol.* **2016**, *7*, 1000346. [[CrossRef](#)]
32. Dasari, S.; Yedjou, C.G.; Brodell, R.T.; Cruse, A.R.; Tchounwou, P.B. Therapeutic strategies and potential implications of silver nanoparticles in the management of skin cancer. *Nanotechnol. Rev.* **2020**, *9*, 1500–1521. [[CrossRef](#)]
33. Yamada, M.; Foote, M.; Prow, T.W. Therapeutic gold, silver, and platinum nanoparticles. *Wiley Interdiscip. Rev. Nanomed. Nanobiotechnol.* **2015**, *7*, 428–445. [[CrossRef](#)]
34. Petropoulos, D.; Worth, L.L.; Mullen, C.A.; Madden, R.; Mahajan, A.; Choroszy, M.; Ha, C.S.; Champlin, R.C.; Chan, K.W. Total body irradiation, fludarabine, melphalan, and allogeneic hematopoietic stem cell transplantation for advanced pediatric hematologic malignancies. *Bone Marrow Transplant.* **2006**, *37*, 463–467. [[CrossRef](#)]
35. Kato, H.; Taji, H.; Ogura, M.; Kagami, Y.; Oki, Y.; Tsujimura, A.; Fuwa, N.; Kodaira, T.; Seto, M.; Yamamoto, K.; et al. Favorable consolidative effect of high-dose melphalan and total-body irradiation followed by autologous peripheral blood stem cell transplantation after rituximab-containing induction chemotherapy with in vivo purging in relapsed or refractory follicular. *Clin. Lymphoma Myeloma* **2009**, *9*, 443–448. [[CrossRef](#)]
36. Spitzer, G.; Jagannath, S.; Dicke, K.A.; Armitage, J.; Zander, A.R.; Vellekoop, L.; Horwitz, L.; Cabanillas, F.; Zagars, G.K.; Velasquez, W.S. High-dose melphalan and total body irradiation with bone marrow transplantation for refractory malignancies. *Eur. J. Cancer Clin. Oncol.* **1986**, *22*, 677–684. [[CrossRef](#)]
37. Chang, S.Y.; Alberts, D.S.; Farquhar, D.; Melnick, L.R.; Walson, P.D.; Salmon, S.E. Hydrolysis and protein binding of melphalan. *J. Pharm. Sci.* **1978**, *67*, 682–684. [[CrossRef](#)]
38. Tian, B.; Hua, S.; Liu, J. Cyclodextrin-based delivery systems for chemotherapeutic anticancer drugs: A review. *Carbohydr. Polym.* **2020**, *232*, 115805. [[CrossRef](#)] [[PubMed](#)]
39. Gidwani, B.; Vyas, A. A Comprehensive Review on Cyclodextrin-Based Carriers for Delivery of Chemotherapeutic Cytotoxic Anticancer Drugs. *Biomed Res. Int.* **2015**, *2015*, 198268. [[CrossRef](#)]
40. Zhang, D.; Lv, P.; Zhou, C.; Zhao, Y.; Liao, X.; Yang, B. Cyclodextrin-based delivery systems for cancer treatment. *Mater. Sci. Eng. C* **2019**, *96*, 872–886. [[CrossRef](#)] [[PubMed](#)]
41. Szejtli, J. Introduction and General Overview of Cyclodextrin Chemistry. *Chem. Rev.* **1998**, *76*, 1825–1845. [[CrossRef](#)]
42. Crini, G.; Fourmentin, S.; Fenyvesi, É.; Torri, G.; Fourmentin, M.; Morin-Crini, N. Cyclodextrins, from molecules to applications. *Environ. Chem. Lett.* **2018**, *16*, 1361–1375. [[CrossRef](#)]
43. Stella, V.J.; He, Q. Cyclodextrins. *Toxicol. Pathol.* **2008**, *36*, 30–42. [[CrossRef](#)]
44. Ma, D.Q.; Rajewski, R.A.; Stella, V.J. New injectable melphalan formulations utilizing (SBE)(7m)- β -CD or HP- β -CD. *Int. J. Pharm.* **1999**, *189*, 227–234. [[CrossRef](#)]
45. Loftsson, T.; Björnsdóttir, S.; Pálsdóttir, G.; Bodor, N. The effects of 2-hydroxypropyl- β -cyclodextrin on the solubility and stability of chlorambucil and melphalan in aqueous solution. *Int. J. Pharm.* **1989**, *57*, 63–72. [[CrossRef](#)]
46. Hari, P.; Aljitawi, O.S.; Arce-Lara, C.; Nath, R.; Callander, N.; Bhat, G.; Allen, L.F.; Stockerl-Goldstein, K. A Phase IIb, Multicenter, Open-Label, Safety, and Efficacy Study of High-Dose, Propylene Glycol-Free Melphalan Hydrochloride for Injection (EVOMELA) for Myeloablative Conditioning in Multiple Myeloma Patients Undergoing Autologous Transplantation. *Biol. Blood Marrow Transplant.* **2015**, *21*, 2100–2105. [[CrossRef](#)]
47. Silva, N.; Riveros, A.; Yutronic, N.; Lang, E.; Chornik, B.; Guerrero, S.; Samitier, J.; Jara, P.; Kogan, M. Photothermally Controlled Methotrexate Release System Using β -Cyclodextrin and Gold Nanoparticles. *Nanomaterials* **2018**, *8*, 985. [[CrossRef](#)] [[PubMed](#)]
48. Mino, R. Caira On the isostructurality of cyclodextrin inclusion complexes and its practical utility. *Rev. Roum. Chim.* **2001**, *46*, 371–386.
49. Sala, A.; Hoossen, Z.; Bacchi, A.; Caira, M.R. Two crystal forms of a hydrated 2:1 β -cyclodextrin \times fluconazole complex: Single crystal X-ray structures, dehydration profiles, and conditions for their individual isolation. *Molecules* **2021**, *26*, 4427. [[CrossRef](#)] [[PubMed](#)]
50. Dang, Z.; Xin Song, L.; Qing Guo, X.; Yun Du, F.; Yang, J.; Yang, J. Applications of Powder X-ray Diffraction to Inclusion Complexes of Cyclodextrins. *Curr. Org. Chem.* **2011**, *15*, 848–861. [[CrossRef](#)]
51. Schneider, H.J.; Hacket, F.; Rüdiger, V.; Ikeda, H. NMR studies of cyclodextrins and cyclodextrin complexes. *Chem. Rev.* **1998**, *98*, 1755–1785. [[CrossRef](#)]
52. Pessine, F.B.; Calderini, A.; Alexandrino, G.L. Review: Cyclodextrin Inclusion Complexes Probed by NMR Techniques. In *Magnetic Resonance Spectroscopy*; Intechopen: London, UK, 2012; p. 264.
53. Higuchi, T.; Connors, K.A. Phase Solubility Techniques. In *Advances in Analytical Chemistry and Instrumentation*; O'Reilly: Sebastopol, CA, USA, 1965; Volume 4, pp. 117–212.
54. Saokham, P.; Muankaew, C.; Jansook, P.; Loftsson, T. Solubility of cyclodextrins and drug/cyclodextrin complexes. *Molecules* **2018**, *23*, 1161. [[CrossRef](#)]
55. Connors, K.A. The stability of cyclodextrin complexes in solution. *Chem. Rev.* **1997**, *97*, 1325–1358. [[CrossRef](#)]
56. Rao, V.M.; Stella, V.J. When can cyclodextrins be considered for solubilization purposes? *J. Pharm. Sci.* **2003**, *92*, 927–932. [[CrossRef](#)] [[PubMed](#)]
57. Herrera, B.; Bruna, T.; Guerra, D.; Yutronic, N.; Kogan, M.J.; Jara, P. Silver Nanoparticles Produced by Magnetron Sputtering and Selective Nanodecoration onto α -Cyclodextrin/Carboxylic Acid Inclusion Compounds Crystals. *Adv. Nanopart.* **2013**, *2*, 112–119. [[CrossRef](#)]

58. Silva, N.; Moris, S.; Herrera, B.; Diaz, M.; Kogan, M.; Barrientos, L.; Yutronic, N.; Jara, P. Formation of copper nanoparticles supported onto inclusion compounds of α -cyclodextrin: A new route to obtain copper nanoparticles. *Mol. Cryst. Liq. Cryst.* **2010**, *521*, 246–252. [[CrossRef](#)]
59. Creighton, J.A.; Eadon, D.G. Ultraviolet-visible absorption spectra of the colloidal metallic elements. *J. Chem. Soc. Faraday Trans.* **1991**, *87*, 3881–3891. [[CrossRef](#)]
60. Chen, M.C.; Yang, Y.L.; Chen, S.W.; Li, J.H.; Aklilu, M.; Tai, Y. Self-assembled monolayer immobilized gold nanoparticles for plasmonic effects in small molecule organic photovoltaic. *ACS Appl. Mater. Interfaces* **2013**, *5*, 511–517. [[CrossRef](#)]
61. Kelly, K.L.; Coronado, E.; Zhao, L.L.; Schatz, G.C. The optical properties of metal nanoparticles: The influence of size, shape, and dielectric environment. *J. Phys. Chem. B* **2003**, *107*, 668–677. [[CrossRef](#)]
62. Mock, J.J.; Smith, D.R.; Schultz, S. Local refractive index dependence of plasmon resonance spectra from individual nanoparticles. *Nano Lett.* **2003**, *3*, 485–491. [[CrossRef](#)]
63. Pestovsky, Y.S.; Srichana, T. Formation of Aggregate-Free Gold Nanoparticles in the Cyclodextrin-Tetrachloroaurate System Follows Finke–Watzky Kinetics. *Nanomaterials* **2022**, *12*, 583. [[CrossRef](#)]
64. Rajamanikandan, R.; Ilanchelian, M.; Ju, H. β -cyclodextrin functionalized gold nanoparticles as an effective nanocatalyst for reducing toxic nitroaromatics. *Opt. Mater.* **2023**, *135*, 113294. [[CrossRef](#)]
65. Park, C.; Youn, H.; Kim, H.; Noh, T.; Kook, Y.H.; Oh, E.T.; Park, H.J.; Kim, C. Cyclodextrin-covered gold nanoparticles for targeted delivery of an anti-cancer drug. *J. Mater. Chem.* **2009**, *19*, 2310–2315. [[CrossRef](#)]
66. Vinita; Tiwari, M.; Prakash, R. Colorimetric detection of picric acid using silver nanoparticles modified with 4-amino-3-hydrazino-5-mercapto-1,2,4-triazole. *Appl. Surf. Sci.* **2018**, *449*, 174–180. [[CrossRef](#)]
67. Tiwari, A.K.; Gupta, M.K.; Pandey, G.; Tilak, R.; Narayan, R.J.; Pandey, P.C. Size and Zeta Potential Clicked Germination Attenuation and Anti-Sporangiospores Activity of PEI-Functionalized Silver Nanoparticles against COVID-19 Associated Mucorales (*Rhizopus arrhizus*). *Nanomaterials* **2022**, *12*, 2235. [[CrossRef](#)] [[PubMed](#)]
68. de Matos, R.A.; Courrol, L.C. Biocompatible silver nanoparticles prepared with amino acids and a green method. *Amino Acids* **2017**, *49*, 379–388. [[CrossRef](#)] [[PubMed](#)]
69. Pan, Y.; Neuss, S.; Leifert, A.; Fischler, M.; Wen, F.; Simon, U.; Schmid, G.; Brandau, W.; Jahnen-Dechent, W. Size-dependent cytotoxicity of gold nanoparticles. *Small* **2007**, *3*, 1941–1949. [[CrossRef](#)]
70. Kansy, M.; Senner, F.; Gubernator, K. Physicochemical high throughput screening: Parallel artificial membrane permeation assay in the description of passive absorption processes. *J. Med. Chem.* **1998**, *41*, 1007–1010. [[CrossRef](#)]
71. Ottaviani, G.; Martel, S.; Carrupt, P.A. Parallel artificial membrane permeability assay: A new membrane for the fast prediction of passive human skin permeability. *J. Med. Chem.* **2006**, *49*, 3948–3954. [[CrossRef](#)]
72. Lopez, C.A.; De Vries, A.H.; Marrink, S.J. Computational microscopy of cyclodextrin mediated cholesterol extraction from lipid model membranes. *Sci. Rep.* **2013**, *3*, srep02071. [[CrossRef](#)]
73. Loftsson, T.; Duchêne, D. Cyclodextrins and their pharmaceutical applications. *Int. J. Pharm.* **2007**, *329*, 1–11. [[CrossRef](#)]
74. Tsinman, O.; Tsinman, K.; Sun, N.; Avdeef, A. Physicochemical selectivity of the BBB microenvironment governing passive diffusion—Matching with a porcine brain lipid extract artificial membrane permeability model. *Pharm. Res.* **2011**, *28*, 337–363. [[CrossRef](#)]
75. Loftsson, T.; Vogensen, S.B.; Brewster, M.E.; Konráósdóttir, F. Effects of cyclodextrins on drug delivery through biological membranes. *J. Pharm. Sci.* **2007**, *96*, 2532–2546. [[CrossRef](#)]
76. Chen, W.; Fan, H.; Balakrishnan, K.; Wang, Y.; Sun, H.; Fan, Y.; Gandhi, V.; Arnold, L.A.; Peng, X. Discovery and Optimization of Novel Hydrogen Peroxide Activated Aromatic Nitrogen Mustard Derivatives as Highly Potent Anticancer Agents. *J. Med. Chem.* **2018**, *61*, 9132–9145. [[CrossRef](#)] [[PubMed](#)]
77. Casamonti, M.; Piazzini, V.; Bilia, A.R.; Bergonzi, M.C. Evaluation of Skin Permeability of Resveratrol Loaded Liposomes and Nanostructured Lipid Carriers using a Skin Mimic Artificial Membrane (skin-PAMPA). *Drug Deliv. Lett.* **2019**, *9*, 134–145. [[CrossRef](#)]
78. Pham, S.H.; Choi, Y.; Choi, J. Stimuli-responsive nanomaterials for application in antitumor therapy and drug delivery. *Pharmaceutics* **2020**, *12*, 630. [[CrossRef](#)] [[PubMed](#)]
79. Tam, K.Y.; Avdeef, A.; Tsinman, O.; Sun, N. The permeation of amphoteric drugs through artificial membranes—An in combo absorption model based on paracellular and transmembrane permeability. *J. Med. Chem.* **2010**, *53*, 392–401. [[CrossRef](#)]
80. Avdeef, A.; Tsinman, O. PAMPA-A drug absorption in vitro model: 13. Chemical selectivity due to membrane hydrogen bonding: In combo comparisons of HDM-, DOPC-, and DS-PAMPA models. *Eur. J. Pharm. Sci.* **2006**, *28*, 43–50. [[CrossRef](#)]
81. Bolaños, K.; Sánchez-Navarro, M.; Giralt, E.; Acosta, G.; Albericio, F.; Kogan, M.J.; Araya, E. NIR and glutathione trigger the surface release of methotrexate linked by Diels–Alder adducts to anisotropic gold nanoparticles. *Mater. Sci. Eng. C* **2021**, *131*, 112512. [[CrossRef](#)]
82. Herrera, B.; Adura, C.; Yutronic, N.; Kogan, M.J.; Jara, P. Selective nanodecoration of modified cyclodextrin crystals with gold nanorods. *J. Colloid Interface Sci.* **2013**, *389*, 42–45. [[CrossRef](#)]
83. Lv, P.; Zhang, D.; Guo, M.; Liu, J.; Chen, X.; Guo, R.; Xu, Y.; Zhang, Q.; Liu, Y.; Guo, H.; et al. Structural analysis and cytotoxicity of host-guest inclusion complexes of cannabidiol with three native cyclodextrins. *J. Drug Deliv. Sci. Technol.* **2019**, *51*, 337–344. [[CrossRef](#)]

84. Slepíčka, P.; Kasálková, N.S.; Siegel, J.; Kolská, Z.; Švorčík, V. Methods of gold and silver nanoparticles preparation. *Materials* **2020**, *13*, 1. [[CrossRef](#)]
85. Hirsch, U.M.; Teuscher, N.; Rühl, M.; Heilmann, A. Plasma-enhanced magnetron sputtering of silver nanoparticles on reverse osmosis membranes for improved antifouling properties. *Surf. Interfaces* **2019**, *16*, 1–7. [[CrossRef](#)]
86. Asanithi, P.; Chaiyakun, S.; Limsuwan, P. Growth of silver nanoparticles by DC magnetron sputtering. *J. Nanomater.* **2012**, *2012*, 963609. [[CrossRef](#)]
87. Omar, S.M.; Ibrahim, F.; Ismail, A. Formulation and evaluation of cyclodextrin-based nanosponges of griseofulvin as pediatric oral liquid dosage form for enhancing bioavailability and masking bitter taste. *Saudi Pharm. J.* **2020**, *28*, 349–361. [[CrossRef](#)] [[PubMed](#)]
88. Rodríguez-Llamazares, S.; Jara, P.; Yutronic, N.; Noyong, M.; Fischler, M.; Simon, U. Preferential adhesion of silver nanoparticles onto crystal faces of α -Cyclodextrin/carboxylic acids inclusion compounds. *J. Nanosci. Nanotechnol.* **2012**, *12*, 8929–8934. [[CrossRef](#)] [[PubMed](#)]
89. Okumu, J.; Dahmen, C.; Sprafke, A.N.; Luysberg, M.; Von Plessen, G.; Wuttig, M. Photochromic silver nanoparticles fabricated by sputter deposition. *J. Appl. Phys.* **2005**, *97*, 094305. [[CrossRef](#)]
90. Ye, Y.; Loh, J.Y.Y.; Flood, A.; Fang, C.Y.; Chang, J.; Zhao, R.; Brodersen, P.; Kherani, N.P. Plasmonics of Diffused Silver Nanoparticles in Silver/Nitride Optical Thin Films. *Sci. Rep.* **2019**, *9*, 20227. [[CrossRef](#)]

Disclaimer/Publisher’s Note: The statements, opinions and data contained in all publications are solely those of the individual author(s) and contributor(s) and not of MDPI and/or the editor(s). MDPI and/or the editor(s) disclaim responsibility for any injury to people or property resulting from any ideas, methods, instructions or products referred to in the content.